Asian Journal of Pharmaceutical Sciences 17 (2022) 544–556

Available online at www.sciencedirect.com

ScienceDirect

journal homepage: www.elsevier.com/locate/AJPS

Original Research Paper

Amphotericin B release rate is the link between drug status in the liposomal bilayer and toxicity

Yuri Svirkin[a], *Jaeweon Lee*[a], *Richard Marx*[a], *Seongkyu Yoon*[b,*], *Nelson Landrau*[a], *Md Abul Kaisar*[c], *Bin Qin*[c], *Jin H. Park*[c], *Khondoker Alam*[c], *Darby Kozak*[c], *Yan Wang*[c], *Xiaoming Xu*[d], *Jiwen Zheng*[e], *Benjamin Rivnay*[a]

[a] *Landrau Scientific Innovations, Leominster, MA, United States of America*
[b] *University of Massachusetts Lowell, Lowell, MA, United States of America*
[c] *Office of Research and Standards, Office of Generic Drugs, Center for Drug Evaluation and Research, U.S. Food and Drug Administration, Silver Spring, MD, United States of America*
[d] *Office of Testing and Research, Office of Pharmaceutical Quality, Center for Drug Evaluation and Research, U.S. Food and Drug Administration, Silver Spring, MD, United States of America*
[e] *Office of Science and Engineering Laboratories, Center for Devices and Radiological Health, U.S. Food and Drug Administration, Silver Spring, MD, United States of America*

ARTICLE INFO

Article history:
Received 12 January 2022
Revised 26 March 2022
Accepted 13 April 2022
Available online 8 June 2022

Keywords:
Amphotericin B
UV–Vis Spectrum
Drug Release
In Vitro Toxicity
Aggregation Status
Liposomes

ABSTRACT

Amphotericin B (AmB) is an amphiphilic drug commonly formulated in liposomes and administered intravenously to treat systemic fungal infections. Recent studies on the liposomal drug product have shed light on the AmB aggregation status in the bilayer, which heat treatment (curing) modifies. Although toxicity was found related to aggregation status - loose aggregates significantly more toxic than tight aggregates - the precise mechanism linking aggregation and toxicity was not well understood. This study directly measured drug release rate from various AmB liposomal preparations made with modified curing protocols to evaluate correlations among drug aggregation state, drug release, and *in vitro* toxicity. UV–Vis spectroscopy of these products detected unique curing-induced changes in the UV spectral features: a ~25 nm blue-shift of the main absorption peak (λ_{max}) in aqueous buffer and a decrease in the OD_{346}/OD_{322} ratio upon thermal curing, reflecting tighter aggregation. *In vitro* release testing (IVRT) data showed, by applying and fitting first-order release kinetic models for one or two pools, that curing impacts two significant changes: a 3–5-fold drop in the overall drug release rate and a ten-fold decrease in the ratio between the loosely aggregated and the tightly aggregated, more thermodynamically stable drug pool. The kinetic data thus corroborated the trend independently deduced from the UV–Vis spectral data. The *in vitro* toxicity assay indicated a decreased toxicity with curing, as shown by the

* Corresponding author.
E-mail address: Seongkyu_Yoon@uml.edu (S. Yoon).
Peer review under responsibility of Shenyang Pharmaceutical University.

https://doi.org/10.1016/j.ajps.2022.04.007

significantly increased concentration, causing half-maximal potassium release (TC_{50}). The data suggest that the release of AmB requires dissociation of the tight complexes within the bilayer and that the reduced toxicity relates to this slower rate of dissociation. This study demonstrates the relationship between AmB aggregation status within the lipid bilayer and drug release (directly measured rate constants), providing a mechanistic link between aggregation status and *in vitro* toxicity in the liposomal formulations.

1. Introduction

Amphotericin B (AmB) is an amphiphilic macrolide antimycotic drug substance comprised of a highly hydrophobic hepta-ene motif and hydrophilic poly-ol and mycoseamine groups [1]. In aqueous media, regardless of surfactant, AmB's ability to self-assemble and create water-soluble toxic aggregates is a well-characterized mechanism [2–8]. AmB aggregation and its dynamics continue to be a convoluted topic due to the simultaneous presence of several different species in mixtures, with an equilibrium that depends on the formulation composition, the solvents, and mode of dilution (*e.g.*, if added to the water) [8–13], the drug concentration and temperature [14,15]. Aggregation in aqueous suspensions formed without heating can be reversible [8,16,17]. Spectral analysis of the drug product in water, or a similar polar environment, shows a typical UV–Vis absorption spectrum of aggregates with a main peak in the low to mid 300 nm. In contrast, the main peak of the monomer is in the low 400 nm region [2,3,7,9,11,18]. Due to its physicochemical nature, AmB also dimerizes and aggregates in detergent or lipid environments.

Aggregation in Lipids. In lipids, the distribution of aggregated species also depends on the total AmB concentration, production/mixing methods, nature of the lipids present, ratios amongst lipids, and the drug to lipid ratio [19–24]. At low AmB to lipid ratios, large aggregates do not form. Instead, large cylindrical structures (driven by molecular polarity) can destabilize the membrane and were suggested as one potential mechanism of AmB toxicity [19]. As found in aqueous media, the absorption spectra of AmB in lipid membranes are also characterized by strong hypsochromism (blue-shift of the main peak from 408 nm to approximately 330–350 nm region), typical for aggregation. Studies suggest that 4–9 AmB molecules form cylindrical aggregate structures [21,25,26] as a possible molecular organization in lipid bilayers. Using fluorescence techniques on dipalmitoylphosphatidylcholine (DPPC) liposomes, without sterol and heat curing, show a preference for monomers compared to dimers at temperatures above the lipid phase transition. Moreover, the data suggest that AmB in the bilayer distributes between two populations: one perpendicular to the plane and the second parallel, perceived to be localized in the polar region of the membrane [27]. At higher AmB concentrations, which promote aggregation, the ratio of aggregate to monomer increases, and so does the relative fraction of the perpendicular orientation [23]. As the understanding of AmB has progressed, it becomes clearer that at low AmB: lipid ratios, the primary species involved in the lipid system(s) are confined to monomers, parallel/anti-parallel dimers, and tetramers which always exist in equilibrium controlled by the physical and chemical conditions [25,28].

Heating. As AmB research progressed, the benefits of temperature curing the AmB formulation were demonstrated for widening the therapeutic window. Several studies identified a phenomenon known as super-aggregation or super-packing, which is induced by extensive exposure to high temperature (> 55 °C) and characterized by further blue-shifting of the main aggregate peak from the mid-300 nm to ~321 nm [20,29,30]. Studies using circular dichroism in aqueous media show that at low concentrations, AmB tends to become less aggregated with temperature [15]. In aqueous suspensions with a surfactant (Fungizone, 70 °C), a qualitative change in configuration occurs upon heating [16], which is reflected by a blue-shift of the main UV spectral peak to 321–322 nm. A similar change was observed by circular dichroism in aqueous medium without the surfactant (<10% DMSO at 50–60 °C) [17]. These changes were interpreted as super-aggregation [31] and were observed with the free drug (in aqueous suspensions) [16], in mixtures with deoxycholate [2,11,29,31-33], deoxycholate colloidal solutions [17], as well as in lipids-containing formulations [30,34,35].

Toxicity. The relationship between toxicity and aggregation status is key to understanding the narrow therapeutic window of AmB formulations. Some of the above studies demonstrated that super-aggregated AmB is less toxic than the loosely aggregated material and that the latter was more toxic than the monomeric form [35,36]. Notably, heat (curing)-induced super-aggregation was beneficial against toxicity in several types of formulations, including surfactant-based (Fungizone) [28,31,35,37,38] and liposomal (AmBisome) formulations [30,39]. Toxicity of lipid formulations was also shown to depend on particle size and lamellarity [40–43], on the nature of and relative concentration of the sterol(s), and the drug-to-lipid ratios [44–46]. Studies on these parameters involved *in vivo* studies (mice or rats), *in vitro* cell lines [47,48] and surrogate toxicity testing systems like potassium release in erythrocytes [28,49], or artificial system models for toxicity [15,50]. While the effects of the lipids on toxicity may be partially derived from influencing the equilibria amongst different aggregate forms in the liposomes, this could also be related to liposome-cell (membrane), liposome-lipoprotein, and liposome-albumin interactions *in vivo* (affecting pharmacodynamics and pharmacokinetics).

Multiple studies reported *in vitro* toxicity by the release of potassium [29,49,51,52] or complete dissociation of the membrane and release of hemoglobin from red blood cells (RBCs) [43,53]. Other toxicity/efficacy mechanisms have also been proposed, such as lipoprotein-mediated transfer [14] or drug-mediated extraction of ergosterol from the fungal membrane [54]. Regardless of the mechanism, the aggregation status and associated toxicity are dependent on the drug concentration. Indeed, concentration-dependent toxicity was well established both *in vivo* and *in vitro* [55].

Despite an abundance of studies on the relationship between drug concentration, aggregation, and toxicity, less has been published on the role of AmB release rates and toxicity. Mehta et al. [56] compared liposomal formulation toxicity on *Candida* or mammalian RBCs, raising the possibility that drug release rates may account for the selectivity and toxicity. In another study, Szoka et al. [46] showed that liposome composition, size, and structure significantly influence *in vitro* toxicity of AmB against murine cells in culture. They show a 2–8-fold difference in toxicity; however, the study did not focus on the state of drug aggregation. The authors in both studies suggested the reduced toxicity was related to the rate of drug transfer to the target membrane but stopped short of measuring drug release rates [46,56]. Peterson et al. [50] also showed that variations of lipid compositions influenced toxicity (potassium release) in target membranes without discussing curing or aggregation. They, too, stated that the drug release rates could be responsible for the variations but did not directly measure drug release rates [50].

The present study directly measures drug release rates in a model system to confirm those previous studies' suggestions that the tight aggregation induced by curing results in slower rates of drug release, providing a possible mechanistic explanation for the reduced toxicity

2. Materials and methods

2.1. Materials

Amphotericin B (Cat: 1397-89-3, Crystal, > 98%, Lot# B16LM06231), (AmB; BOC Sciences, Shirley, NY), Bovine Serum (Gibco/Thermofisher Scientific, New Zealand), Chloroform (Alfa Aesar, Haverhill, MA), Cholesterol (Sigma, St. Louis, MO), γ-Cyclodextrin (Xian Geekee Biotech Co., Shaanxi, China), Di-Stearoyl-Phosphatidyl-Glycerol (DSPG; Lipoid, Ludwigshafen, Germany), Hydrochloric Acid (HCl; Sigma, St. Louis, MO), Hydrogenated Phosphatidylcholine from Soybean (HSPC; Lipoid, Ludwigshafen, Germany), Isopropyl Alcohol (IPA; Duda Diesel LLC, Madison, AL), Methanol (Spectrum Corp, Gardena, CA), NaOH Pellets (Spectrum Corp, Gardena, CA), Potassium standard solution (Cole-Parmer, Vernon Hills, IL), Sprague Dawley Rat Whole Blood (Cat: RAT00RBCNHPZN, BioIVT, Baltimore, MD), Sodium Chloride (Aldrich Chemical, Milwaukee, WI), Sodium Succinate (SS; Spectrum Chemical, Gardena, CA), Sucrose (EMD Millipore Corp, Burlington, MA), Tocopherol (EMD Millipore Corp, Burlington, MA), Ultrapure Succinic Acid (Spectrum Chemical, Gardena, CA) and Water (18 Megaohm, in-house prepared, Leominster, MA).

2.2. AmBisome-like formulations

AmBisome-like formulations were prepared following Example 1 in the innovator's disclosed patent document [57], with added details gleaned from an earlier publication [30]. Specific variations in the formulation excipients or process were attempted to explore their effects on toxicity and the biophysical features of the products. Details on these variations are specified in the respective results and discussion section. The manufacturing process is comprised of four steps. In step I, AmB drug substance was mixed in a glass vessel with lipid excipients (HSPC, DSPG, Cholesterol, and the antioxidant Tocopherol). The first step was carried out at 65 °C to facilitate the dissolution of the saturated lipids. The acidification of DSPG was critical to allow AmB solubilization which was visually detectable as a transition from an orange suspension to a dark tea-color solution. Step II (immediately following) involved spray drying the organic solution, yielding a yellowish powder stored at −20 °C until further processing. Specifically, the resulting solution from step I was dried using a spray drier (Buchi Mini B190, BUCHI, Cleveland, OH). The processed solution was pumped (Model QVG50 Lab Pump and Model V200 Stroke Rate Controller, Fluid Metering Inc., Syosset, NY) at 1.2 ml/min into the spray dryer, with inlet and outlet temperatures of 52 °C and 44 °C, respectively, using nitrogen as the atomizing gas (600 L/h) and 92% aspiration for drying. Most spray drying processes were conducted at ambient temperature (26 °C). Step III involved hydrating the resultant powder from step II to an AmB concentration of ∼3–4 mM with a sucrose succinate buffer (7.5%, w:v sucrose, 10 mM succinate buffer pH 5.5) and heating to 55 °C. The hydrated solution is then sonicated and homogenized for 2 cycles of 90–100 psi shearing force (PL-60 Shear Jet, Dyhydrodynamics, Maynard, MA). Single unilamellar vesicles (SUVs) in the range of 90–150 nm diameter were routinely obtained. The resultant liposome suspension was then cured (65 °C for 6 h, unless otherwise specified) in a hot water bath (Lauda Type B Immersion Circulator, Lauda, Lauda-Königshofen, Germany). Aliquots were taken for various analytical characterizations and either refrigerated with 0.01% sodium azide (short term) or further processed with lyophilization. In a typical lyophilization cycle for step IV, the material was frozen to −40 °C by a ∼−0.5 °C/min ramp and then annealed to −27 °C for 2 h. The primary drying occurred at −20 °C and 60 mTorr, with secondary drying at 40 °C and 60 mTorr. All lyophilization runs were carried out with 6 ml fills in 10 ml clear glass vials (60-vial total per run) using a VirTis AdVantage Pro (SP industries, Warminster, PA).

2.3. Spectral analysis by UV–Vis spectroscopy

For quantitative analysis, test articles were quantified by 1:80 (v:v) dilution in methanol. Dilutions of >1:65 were necessary to obtain the reproducible spectrum typical of monomers. Specimens were incubated for 30 min at room temperature to allow for complete dissolution. AmB concentration was derived from the OD_{405} using 150,000 OD/(mol·cm) as the molar extinction coefficient [49]. Spectra were measured on the Agilent spectrophotometer (Agilent 8453 G1103A, Agilent Technologies, Santa Clara, CA) in a 1 cm light path quartz

cuvette. The instrumental resolution was 1 nm. Since the AmB concentrations following a dilution in methanol were ~1 log lower than the maximum solubility in methanol, these spectra reflected fully soluble AmB and were identical for all tested samples, regardless of the origin. Dilutions of aqueous suspensions at <1:65 (v:v) in methanol were avoided due to spectral shifts indicative of aggregation, typical for transitioning to an aqueous environment.

For qualitative analysis, based on the calculated stock concentrations, the test specimens and the standards (AmBisome) were diluted to 10–20 μM in sodium succinate buffer. The absorption spectrum was collected for each sample between OD_{300}–OD_{450} with 1 nm steps. Three parameters were extracted for product characterization: (1). λ_{max} (main peak position, PP), (2). main peak ratio (MPR, OD_{346}/OD_{322}) and (3). peak ratio (OD_{415} /OD_{322}). 415 nm was partially representative of AmB monomers. Typical values for these three parameters in AmBisome were ~321 nm, ~0.28 and ~0.13, respectively. OD_{500} was subtracted as background noise. Since the spectra of uncured formulations show absorption in the main peak position of the fully cured formulations, and the fully cured material (*e.g.*, AmBisome) also absorbs in the position of uncured formulations, mutual corrections were necessary to optimize the representation of aggregate populations. This correction (translating OD to molarity) assumes similar molar extinction of both species (not independently confirmed) and was implemented as follows:

$$\frac{OD_{346}}{OD_{322}} = \frac{OD_{346M} - OD_{322M}\left(\frac{OD_{346\ AmBisome}}{OD_{322\ AmBisome}}\right)}{OD_{322M} - OD_{346M}\left(\frac{OD_{322\ Unc}}{OD_{346\ Unc}}\right)}$$

Where, OD_{346}/OD_{322} is the corrected main peak ratio, OD_{346M}, and OD_{322M} are the measured raw UV absorbances of the evaluated formulations at the respective wavelengths. Correction reference preparations (uncured (Unc) or commercial AmBisome) were employed as specified in the formula. This correction assumes OD_{346}/OD_{322} remains constant at different concentrations. No pure forms of the loose or tightly aggregated species are available. Therefore, even the corrected values need be carefully considered as they offer the best available approximate corrections. Average triplicate measurements were used for the determination of UV absorbances of AmBisome and uncured formulations.

2.4. *In vitro drug release test (IVRT)*

This IVRT was adopted from the recent paper by Tang et al. [58]. The test is based on a closed-loop USP Apparatus 4 (CE7 Smart 8000–2, Sotax, Basel, Switzerland). The system was composed of a dissolution tester, a multi-channel dispenser (IPC High Precision Multi-Channel Dispenser ISM931C, ISMATEC®, Wertheim, Germany), and a UV–Vis spectrophotometer (Agilent 8453, G1103A, Agilent Technologies, Santa Clara, CA). The dissolution tester can test 7 samples simultaneously; 2 flow-through cells were used for the reference (RLD, AmBisome) and the control (free AmB), which were used to determine the maximal expected concentration in each formulation.

Dialysis Membrane Preparation: Six dialysis membranes (Spectra/Por® Float-A-Lyzer®G2 300 kDa MWCO, G235036, Repligen Corp., Rancho Dominguez, CA) were pre-conditioned with 10% (v:v) IPA water before each run. Briefly, the membranes were filled with and then incubated in 1 l 10% IPA in water on a magnetic stirrer plate (Ret Control-Visc RETCVS1, IKA, Staufen, Germany) for 2 h at 50 rpm. Subsequently, the membranes were rinsed by submersion in 1 l DI water on a magnetic stirrer at 50 rpm overnight (12 h) to remove chemical residuals on the membranes. Exposure of the membranes to air was avoided.

Assay Conditions: Specimen volumes of 1.5 ml were loaded per cell at an API concentration of 0.5 mM (yielding 9.375 μM final concentration). Unless otherwise specified, sink buffer was IVRT buffer (10 mM HEPES, pH 7.4, 5% sucrose) plus 5% γCD, total flow volume per cell was 80 ml, the flow rate was 16 ml/min, and buffer temperature was maintained at 55 °C.

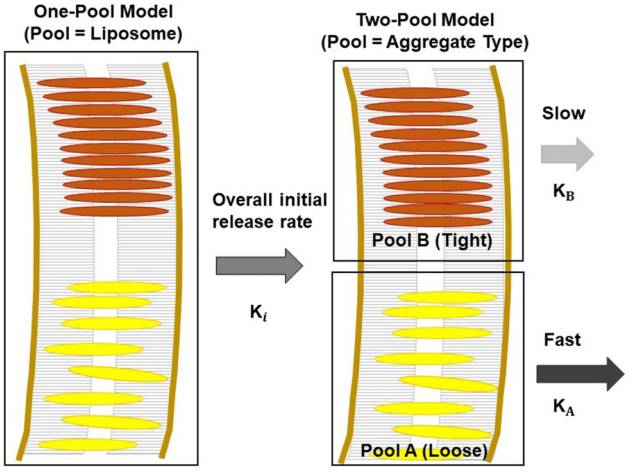

Fig. 1 – One-pool and two-pool models of API release. One-pool considers the liposome the compartment, whereas the two-pool, represents loosely aggregated AmB as pool A and tightly aggregated AmB as pool B. Analysis by two-pool model provides the individual aggregate pool sizes and drug release rate constants from each pool.

Data Capture and Analysis: Absorbance at 415 nm (typical of the γCD-AmB complex) was measured in-line in a 1 mm light path quartz cell with data collected at pre-scheduled intervals. The monomer spectra in water, methanol, serum and γCD all have main peaks in the 405–415 nm region [2,58,60]. Data were processed offline as described in the results and discussion. MATLAB software was utilized to find the IVRT rate constants for the one-pool model (the pool being all liposome-incorporated AmB, see left part of Fig. 1), using Eq. 1:

$$C = C_o e^{-K_i t} \quad (1)$$

Where, C is the released AmB concentration at given time t, C_o the initial AmB concentration and K_i the initial rate constant. Only the initial data sets (10–75 min) were used for obtaining the initial release rate constants in the one-pool analyses. See rationale under results and discussion.

In addition, we evaluated a two-pool/population model (where pool A is the loosely aggregated AmB and pool B is the tightly aggregated AmB within the bilayer, see right part of Fig. 1). This expression followed Eq. 2. Optimizing parameters C_A, C_B, K_A and K_B in Eq. 2:

$$C = C_A e^{-K_A t} + C_B e^{-K_B t} \quad (2)$$

Where C is the released AmB concentration at given time t, and C_A and C_B are the initial concentrations of the two pools, *i.e.*, pool A and pool B. K_A and K_B are *in vitro* release rate constants from pool A and pool B, respectively, and t is the drug release time in h. Fig. 1 depicts the concept of one or two compartments in liposomal AmB.

Release in bovine serum was tested by mixing the drug product (12 μM) in 50% bovine serum in IVRT buffer (no γCD) for up to 7 d at 37 °C. Drug release was followed by tracking the increments in 415 nm absorbance and the increases to the 415 nm/main peak absorbance ratio in the incubation mixture without any separation. AmBisome was used as a reference.

2.5. *In vitro toxicity test*

The *in vitro* toxicity of test articles and standards was assessed using RBCs from rats for an *in vitro* potassium release assay [49]. In a typical experiment, 40 ml RBCs were washed (2000 rpm, 15 min, at 20 °C, SORVALL® RT6000B, Dupont, Wilmington, DE) 4 times in saline, then once in phosphate buffered saline (PBS, pH 7.4) to remove residual free potassium from the medium (potassium levels were also measured at the end of the washing steps). The final pellet was suspended in PBS, cell concentration was assessed (Hemocytometer DHC–N01–5, Incyto, Cheonan-si, Chungnam-do, Republic of Korea) using a light microscope (Olympus BX51, BX51TRF, Olympus, Shinjuku, Tokyo, Japan), and the stock suspension was brought to 5×10^8 RBCs/ml. Following quantitation of the drug in test articles by methanol spectra, API concentration was brought to 200 μg/ml. The stocks were serially diluted to generate 11 concentrations between 0.1953 and 200 μg/ml. Aliquots of 1750 μl from each sample were placed in 15 ml polypropylene tubes, and 250 μl volume of washed RBCs were added to each tube (time 0). The tubes were incubated (VWR relative humidity chamber 9000 L, VWR International, Radnor, PA) for 4 h at 37 °C with constant rocking (4.5 rpm, Vari-Mix™ M48725, Barnstead Thermolyne, Ramsey, MN). The tubes were centrifuged for 10 min at 2000 rpm following incubation and the supernatants decanted (with the release period ending upon the separation). Potassium concentrations were measured using a potassium-specific electrode (Ion-Selective Electrode EW-27,502–39, Cole-Parmer, Vernon Hills, IL). The samples' measured electric potential (mV) was translated to potassium concentrations using a commercial potassium standard (0.315–1000 ppm). Maximum potassium release was defined by the samples incubated with 200 μg/ml free AmB. Relative toxicities were derived from the plot of drug concentration vs. % K^+ release curves and were defined by the drug concentrations inducing half-maximum potassium release, TC_{50} [49]. The curves were analyzed for a sigmoidal and normalized curve fitting, and the TC_{50} values were determined using Prism (GraphPad, ver. 9). Because an increase in TC_{50} signals reduced toxicity, the reciprocal of TC_{50} (*i.e.*, $1/TC_{50}$) was used for further analysis as it directly correlated with the toxicity. *In vitro* toxicity measurements were normalized to reference AmBisome formulations analyzed with each set and defined as $1/TC_{50}$ Norm ($TC_{50(AmBisome)}/TC_{50(test)}$) to overcome batch variability issues.

3. Results and discussion

Curing was previously identified as a critical process for preparing liposomal AmB formulations [30]. The current study evaluated the impact of curing on three fundamental properties: UV–Vis absorption spectra, drug release kinetics under sink and physiological conditions, and *in vitro* toxicity. Multiple formulations were prepared using variations in the curing conditions (time and temperature) for these analyses.

3.1. *Spectral parameters and aggregation*

Fig. 2A shows the spectra of in-house produced formulations. Three significant changes were associated with the curing process: (1) the prominent peak in uncured preparations (345–350 nm) underwent a blue-shift to 321–322 nm (see Section 1); (2) the main peak became narrower, suggesting a more homogeneous population; and (3) the peak intensity at ~415 nm decreased. Therefore, the curing progression was followed by tracking the position of the main peak (λ_{max}) and the absorbance ratio of OD_{346}/OD_{322} (MPR). There is a discrete spectrum with ~345 nm main peak in the loosely aggregated API [21,25,26] and another with a ~322 nm peak for the tightly aggregated API [16,17,31]. Therefore, the main peak ratio can estimate the ratio between the pool/population size of the loose and tight aggregates.

Fig. 2C demonstrates the change in main peak position, and Fig. 2D shows the main peak ratio, both as a function of time under different curing temperatures. The figures show that the tight aggregation (as reflected in decreases of both parameters) was only achieved when curing temperatures were above 55 °C. The changes follow two-phase kinetic behavior where most of the shift was completed within 30 min, followed by a slower process that lasted several hours. The temperature dependence of the spectral values obtained after 6 h of curing is shown in Fig. 2B.

Curing caused a UV–Vis spectrum blue-shift, attributed to changes in the AmB aggregation state within the lipid bilayer. This change led to more AmB in tight aggregate(s), enabling drug aggregate reorganizations otherwise not thermodynamically permitted at lower temperatures.

Some variations are apparent between the formulation or preparation process in the current study and those in earlier publications on liposomal AmB systems. Two main aspects deserve discussion for better understanding the relation between curing and aggregation status in the final drug product.

(1) *Drug load vs. curing*: With 0.5%–25% AmB:lipid mole ratios, the nature of aggregation was sensitive to the relative concentration of drug in the liposome.

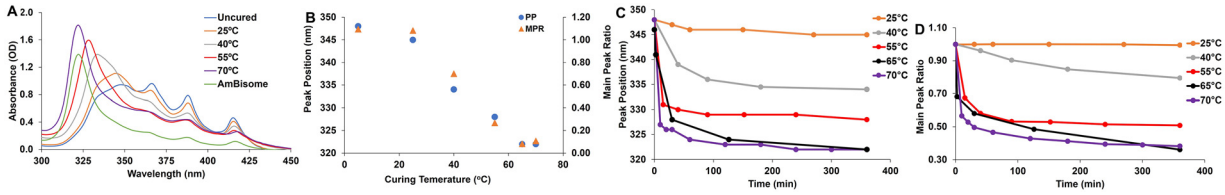

Fig. 2 – (A) UV–Vis spectra, (B) changes in peak position and main peak ratio of specimens cured for 6 h at different temperatures: uncured control (blue); 25 °C (orange); 40 °C (gray); 55 °C (red); 70 °C (violet) and AmBisome (green). Identical concentrations used for in-house preparations. AmBisome, not part of experiment, was added for spectrum shape comparison. (C) peak position and (D) main peak ratio of specimens cured at different temperatures: 25 °C (orange); 40 °C (gray); 55 °C (red); 65 °C (black) and 70 °C (violet).

Aggregation increased with concentration. However, even at the higher end of the specified concentration range [20,23], the main absorbance peak never blue-shifted below 340–350 nm in uncured preparations. 14% (mol), as in the current study (or AmBisome), seems to be around the saturation as liposomal structural features were lost beyond this ratio, *e.g.*, at 25% [20]. Hence, despite maximizing concentration, the aggregate forms induced by overloading the liposome are different than those achieved by heating, where the main peak blue-shift to 320–322 nm was observed.

(2) *Curing temperature and duration*: The curing temperature and duration are essential as the curing process follows two-phase kinetics (Fig. 2C&2D) with a second phase that lasts several hours. Indeed, published spectroscopic studies on specimens at elevated temperatures but without deliberate, prolonged incubations suggest only partial curing occurred. For example, at 64 °C (the short incubation time not specified), only an incomplete blue-shift to 332 nm [27] occurred, but at a much higher temperature (*e.g.*, 80 °C), the peak entirely shifted to 322 nm.

Two temperature-related phenomena should be evaluated in this context:

The lipid phase transition is less critical: Spectra with a peak absorbance at 320–322 nm were reproducibly obtained under the current curing protocol (65–70 °C, 6 h). This temperature is ~25 °C above the phase transition temperature of DPPC (low 40s). However, curing was not completed even at 55 °C, well above the phase transition temperature. Furthermore, literature shows that at high drug:lipid ratios, phase transition disappears, as reported on the obliteration of the DSC phase transition endotherm of DPPC [20] and the loss of cooperativity in the change of the absorption maxima and EPR parameters, upon heating [21,24]. Combined, these arguments rule out that heat is required to bring the bilayer above the (non-existent) lipid phase transition temperature or that the gel-to-liquid transition plays a significant role in the curing process.

Diffusion rates are also less significant: First, at high drug:lipid ratios, the liposome is already at a saturation state (maximal AmB load, see argument 1 above), thus, precluding the existence of a 'bulk' membrane domain in which monomers or aggregates can diffuse. Second, if diffusion was an essential factor in the process, curing could take longer to complete at 45–55 °C. However, the observation that the final spectral features tend to plateau at these suboptimal temperatures rather than slowly approach similar values achieved with specimens cured at >55 °C (see Fig. 2C) further supports the argument marginalizing the role of diffusion as the mechanism underlying curing. Namely, the heat is not required to accelerate re-equilibration by enhancing AmB diffusion in the bilayer.

However, the extended heat delivered while curing could result in altered equilibria (reversible aggregation [17,59]) or re-distribution amongst the different drug aggregate species. The potential also exists for additional forms yet to be described, and therefore the discussion on the ultimate organization of AmB in pharmaceutical drug products remains open.

Nonetheless, recent physicochemical studies provide a thorough analysis defining some of the more abundant membrane-embedded AmB forms [23,25,27]. Therefore, the assignments of loose or tight aggregates should be interpreted in context with the forms proposed in these studies. Specifically, what has been dubbed 'tight aggregates' based on spectral feature may now be identified as larger oligomers (*e.g.*, tetramers), whereas the 'loose aggregates' – as monomers/dimers. Similarly, with the demonstration that a large portion of the membrane-embedded AmB is oriented perpendicular to the plane of the membrane [25,27], the tight aggregate pool may be identified with this fraction, whereas the loose aggregates may include drug molecules oriented parallel to the plane of the membrane. Hence, although Fig. 1 models were employed in this study, given these recent studies, an alternative depiction can be perceived, shown in Fig. 3, whereby curing promotes the left-to-right transition, showing a shift from an orientation parallel to the plane of the membrane to a perpendicular one, and showing monomers/dimers converting to higher oligomers as curing proceeds. As was shown earlier [25], an increase in AmB:lipid ratio was also associated with the shift in orientation from parallel to perpendicular.

Cumulative data suggest that qualitative changes (*i.e.*, formation of new types of aggregates) occur in addition to dynamic re-equilibration amongst the basic forms upon heating. The observation supports the notion that drug overloading does not induce the ultimate main peak blue-shift to 320–322 nm and the demonstrated high stability of the cured species (spectral features induced by curing are

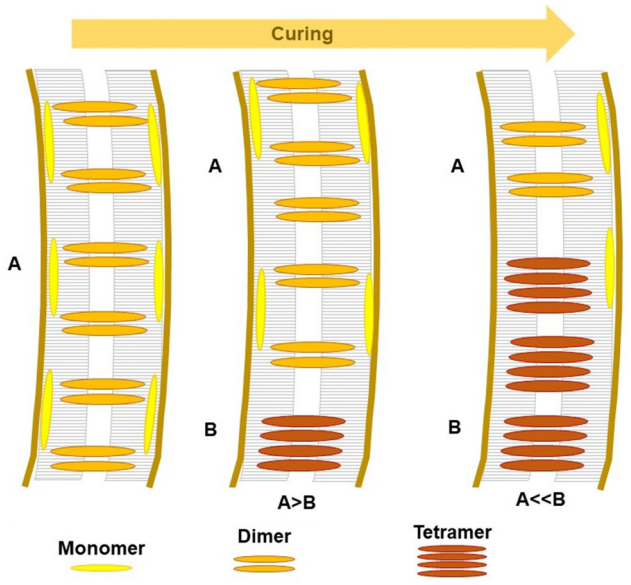

Fig. 3 – Depicts the impact of curing on AmB orientation and aggretation in the liposome bilayer.

stable for months under refrigeration). Elevated temperatures may provide the higher activation energy required for driving the formation of such structures. The feasibility of forming hexamers and octamers [27] or nonamers [21] has been comprehensively evaluated. Likewise, linear strings of AmB in the membrane were demonstrated [27]. Thus, heating may impact the balance between linear and circular (pore-forming) complex formation. Finally, the interaction of other formulation lipids (*e.g.*, cholesterol and phosphatidylglycerol) with the drug in specific aggregate forms could be modified upon heating. Further studies are required to identify and characterize such aggregate forms, particularly in liposomes with a saturating AmB load, in the presence of DSPG and cholesterol, and following extended curing (as used in this study).

3.2. *Kinetic parameters of AMB release*

IVRT was performed on various formulations to determine the impact of aggregates (*i.e.*, loose aggregates *vs.* super-aggregates) on the drug release rate. Fig. 4A shows the increase in cumulative percent release of these preparations for the initial time segment and Fig. 4B – one-pool, first-order fitting for the initial period.

The one-pool model (depicted on the left side of Fig. 1) was selected for analysis confined to the early time segment, yielding the overall initial release rate (K_i) of AmB from the liposome. Fig. 5 provides the rationale behind using only the early phase, showing that the excellent correlation between calculated values and experimental data found for the first 75 min (R^2=0.9997, Fig. 5A) is reduced when fitting data from the entire 24 h period (R^2=0.5583, Fig. 5B).

Indeed, fitting the early release data (first 75 min) of all formulations in this experiment to the first-order (one-pool) release model yielded straight lines with high linear

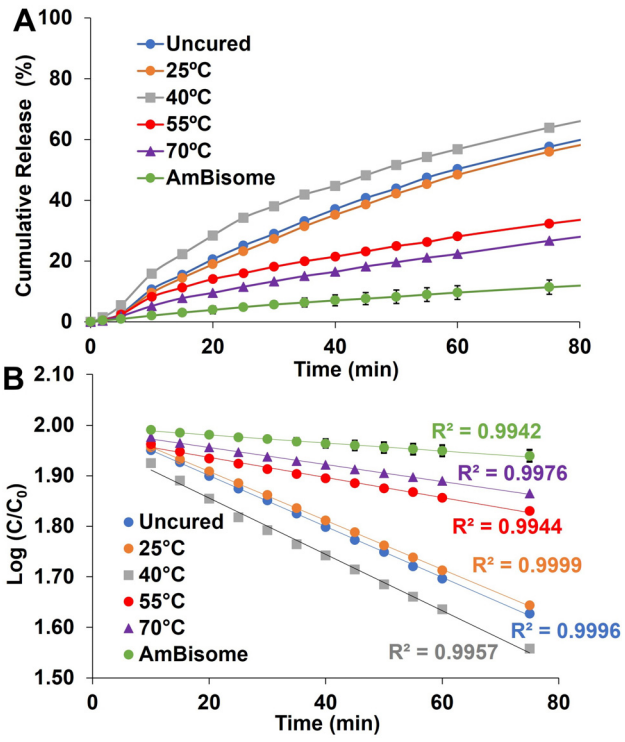

Fig. 4 – IVRT using γCD -containing buffer. Specimens were cured for 6 h at different temperatures: uncured control (blue); 25 °C (orange); 40 °C (gray); 55 °C (red); 70 °C (violet). AmBisome (green): (A) Cumulative release percentage. (B) One-pool first-order fitting for the initial period.

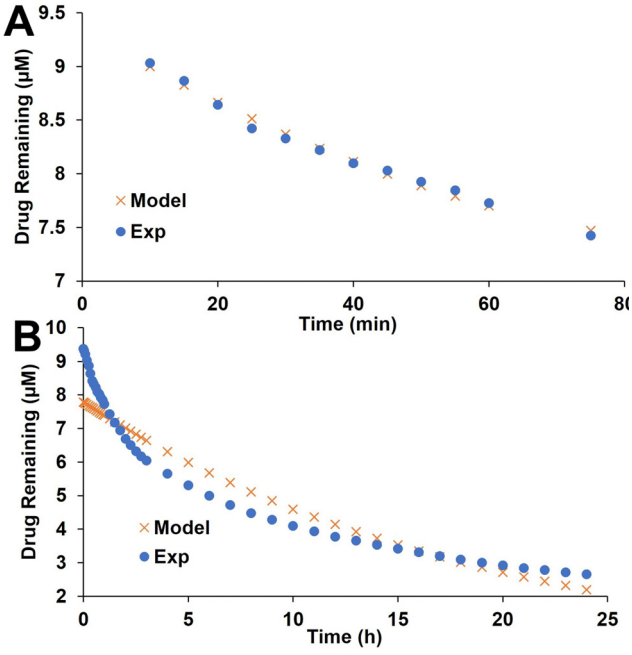

Fig. 5 – One-pool, first-order release curve fitting: (A) Initial 75 min (R^2=0.9997). (B) Full 24 h (R^2=0.5583).

Table 1 – One-pool, first-order release rate constants and correlation coefficients for two different early time segments. All samples were cured for 6 h. Each data set is derived from one Sotax cell compartment. All 5 sets were simultaneously executed with free AmB and AmBisome as controls.

Curing Temperature (°C)	10–75 min		2–4 h		Change (%)
	R^2	K_i	R^2	K'	$100(K_i\text{-}K')/K_i$
Uncured	0.9996	0.6960	0.9982	0.6157	12
25	0.9999	0.6695	0.9937	0.5224	22
40	0.9957	0.7696	0.9996	0.7500	3
55	0.9944	0.2751	0.9827	0.1606	42
70	0.9976	0.2330	0.9640	0.1393	40
AmBisome	0.9942	0.1098	0.9862	0.0634	42

correlation coefficients (R^2>0.994, Fig. 4B), from whose slopes initial rate constants (K_i) were derived. When data from the subsequent 3 h segment (after the first hour) were processed with the same type of analysis, slightly lower linear correlation coefficients were obtained, particularly for the fully cured preparations (R^2>0.96). Table 1 depicts the change in K_i with curing temperature for the formulations 6 h cured and the two time-segments analyzed. As curing temperatures increased, most apparent as temperatures exceeded 55 °C, there was a ~3-fold decrease in K_i (*i.e.*, from 0.6960 in uncured specimens to 0.2330 in samples cured at 70 °C, Table 1), suggesting that cured material as a whole is more resistant to aggregate dissociation and API release. The lowest value was obtained with commercial AmBisome (K_i=0.1098/s).

The differences between K_i and K' most likely indicate significant additional curing during the IVRT analysis (carried at 55 °C). Both observations, the poor fit between model and experimental data (Fig. 5B), and the differences between K_i and K' derived from the one-pool analysis (Table 1) suggest that a two-pool model may better characterize the AmB release kinetics. This model suggests that AmB may exist in two different aggregate forms (loose and tight) as deduced from spectral analyses.

The two-pool model is expressed by Eq. 2 and is depicted in the right part of Fig. 1 (see methods), and it introduces both the sizes (as concentration) of each aggregate pool and the respective IVRT drug release rate constants. Fig. 6 shows the release kinetics from one formulation (cured for 30 min), with the data fitting the two-pool model. Unlike release kinetics in the one-pool model, where only the initial data set yielded a good fit, an excellent fit was observed between the experimental and the calculated data, yielding a correlation coefficient (R^2) of 0.9919 for the complete 24 h set, supporting the two-pool model assumption. This model allows the evaluation of both the release rate constants (K_A and K_B) and the relative sizes of the two aggregate pools (C_A and C_B). The two aggregate-pool model was applied to a study on the time course of curing (0–6 h) at a fixed temperature (65 °C). Table 2 and Fig. 7 show the change of the four parameters in time.

A decrease in the C_A/C_B ratio was calculated with the two-pool model (*e.g.*, a drop from 2.857 to 0.298), as shown in Table 2. This trend is in agreement with the UV-Vis spectral data (Fig. 2D, above), suggesting that as curing progresses, material from pool A (loosely aggregated pool) shifts to pool B (tightly aggregated) (Table 2 and Fig. 7). Fig. 7 shows the changes in time of the two discrete aggregate pools (expressed as concentration), indicating that the tight pool increases at the expense of the loose aggregate pool (as the total drug concentration remains fixed at 9.3 mM in this experiment).

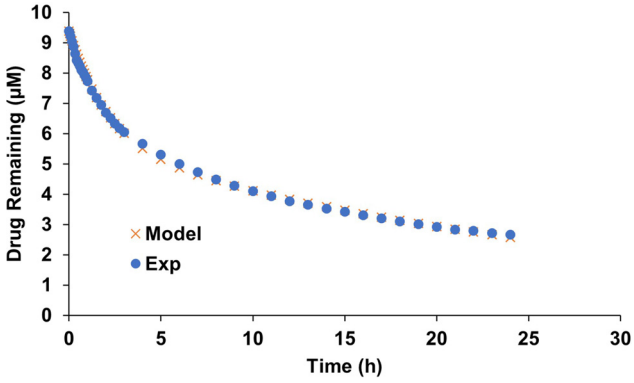

Fig. 6 – Two-pool, first-order release 24 h curve fitting. Specimen was cured for 30 min The different pools are expressed as the molar concentration of the drug in each species of aggregate. Excellent R^2 values were obtained for all specimens in this experiment (Table 2).

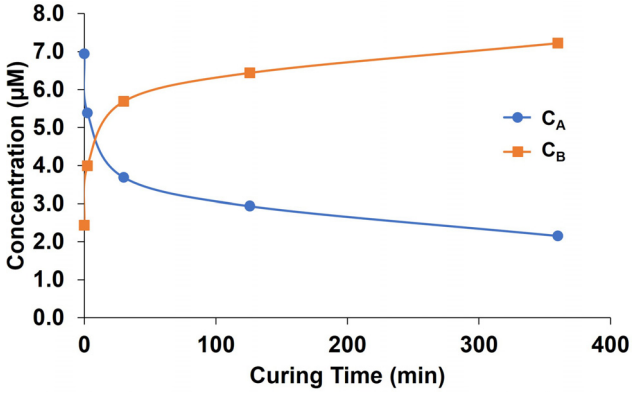

Fig. 7 – Effects of curing time on aggregate pool size calculated using two-pool kinetics. Blue – loosely aggregated pool, C_A; Orange – tightly aggregated pool, C_B.

Table 2 – Aggregate pool size and kinetic release rate constants from the two-pool model derived for specimens cured at 65 °C*.

Kinetic Parameters	Curing Time (min)					
	0	2.5	30	126	360	AmBisome
C_A	6.945	5.384	3.689	2.934	2.154	0.773
C_B	2.431	3.991	5.686	6.441	7.221	8.602
K_A	0.438	0.425	0.485	0.610	0.680	0.773
K_B	0.067	0.032	0.033	0.044	0.024	0.033
R^2	0.835	0.986	0.992	1.000	0.997	0.999
C_A/C_B	2.857	1.349	0.649	0.456	0.298	0.090
K_A/K_B	6.509	13.433	14.660	13.733	28.331	23.148

*C_A, C_B (μM) – aggregate pool sizes (total drug concentration was 9.3 μM), K_A, K_B – release rate constants for the two pools. A – loose-aggregate pool, B – tight-aggregate pool. AmBisome was analyzed as a reference drug product.

In addition, and as expected, the release rate from the tightly aggregated pool B (K_B) was ~ 10–25-fold slower than the release from loose aggregate pool A (see Table 2, K_A, K_B, K_A/K_B). Good R^2 values were found for all time points (Table 2). Notably, some changes in the values of the two rate constants (K_A and K_B) were observed as curing progressed. This may be because the employed model (Eq. 2, see methods) does not account for possible re-equilibrations between pools A and B during the 24 h of the assay.

In summary of the kinetic part, two methodological approaches (spectral and kinetic) and two experimental approaches (temperature- and time- dependence of curing) show excellent agreement with a significant increase in the tight aggregate pool upon curing.

3.3. *In vitro toxicity*

Fig. 8A shows the percentage of potassium released from RBCs with increasing drug concentrations. Two specimen groups are evident in this figure. The first group exhibited lower *in vitro* toxicity, including the AmB (green) and two formulations cured at high temperatures (red and violet). The second group of samples exhibited higher *in vitro* toxicity, including uncured (blue) or partially cured (gray and orange) samples.

The data show that the dose-response curves of fully cured specimens shifted towards lower toxicity (3–5-fold higher TC_{50} values). The reciprocal of TC_{50} ($1/TC_{50}$) was used to provide a more intuitive alignment of higher values with higher toxicities and positive slopes for the different correlations. In addition, the reciprocal toxicity was normalized to AmBisome tested with the samples in the same run ($TC_{50(AmBisome)}/TC_{50(test)}$), introducing a partial correction for the inter-assay variation (see Section 2.5). Using this transformation, Fig. 8B shows the decrease in toxicity with curing temperatures, yielding a profile reminiscent of Fig. 2B above. These data are consistent with our earlier study [30].

Plots of the *in vitro* toxicity *vs.* the UV–Vis spectral and kinetic parameters from the IVRT were done to evaluate correlations. These correlations remove the original variable (*e.g.*, curing time, temperature) from the displayed figure and only show correlations between the measured features. Excellent linear correlations were found between normalized

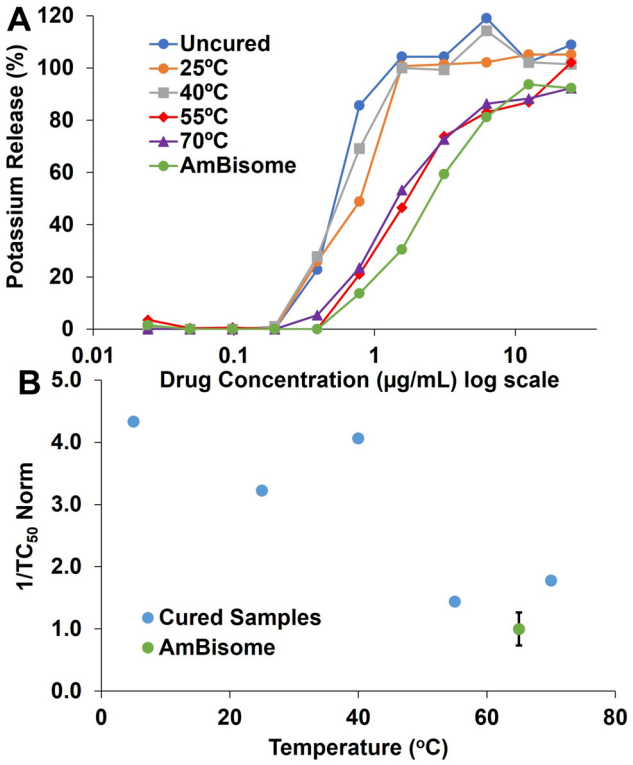

Fig. 8 – Curing effect on *in vitro* toxicity. Specimens were cured for 6 h at different temperatures: uncured control (blue); 25 °C (orange); 40 °C (gray); 55 °C (red); 70 °C (violet) and AmBisome): (A) Potassium release% from RBCs. (B) Reciprocal of *in vitro* toxicity (normalized) dependence on curing temperature. AmBisome ($1/TC_{50}$) values mean of 3 measurements ± SD ($n = 1$).

in vitro toxicity and the main peak ratio, OD_{346}/OD_{max} (Fig. 9A, R^2=0.9912) and peak position (Fig. 9B, R^2=0.9731) for formulations cured at 65 °C (in the time course experiment). Here, OD_{max} is the maximum absorbance value between 318 and 322 nm, with most cases being 322 nm. Linear regression coefficients also showed good agreement between toxicity and spectral parameters for formulations cured for 6 h (in the temperature dependence experiment) with R^2=0.8431 and

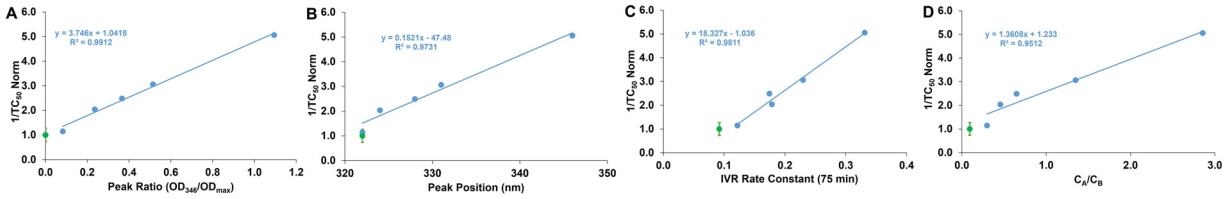

Fig. 9 – *In vitro* toxicity (normalized) correlation with (A) main peak ratio (OD_{346}/OD_{max}), (B) peak position, (C) one-pool IVRT rate constants and (D) two-pool C_A/C_B ratios. Specimens cured for various time at 65 °C. Each point is derived from a separate curing time. AmBisome ($1/TC_{50}$) reference values are shown as green circles and are the mean of 3 measurements ± SD ($n = 1$).

R^2=0.8576 for main peak ratio and peak position, respectively (data not shown).

Similarly, excellent linear correlations were found between normalized *in vitro* toxicity and the initial rate constant (one-pool model, Fig. 9C, R^2=0.9811) and the C_A/C_B ratio (two-pool model, Fig. 9D, R^2=0.9512). Linear regression coefficients also showed a good correlation between toxicity and the kinetic parameters for 6 h cured formulations (the experiment on temperature-dependence) with R^2=0.9067 and R^2=0.7496 for the initial release rate (first-order, one-pool model) and the C_A/C_B pool ratio (first-order, two-pool model), respectively (data not shown).

Thus, the increase in tight aggregates significantly slowed down the liposome's drug release rate, culminating in reduced *in vitro* toxicity [30,32]. The rate of AmB release is likely the link between the observed change in aggregation status and the attenuation of toxicity. Toxicity occurs when drug concentrations exceed a specific threshold. The faster the AmB is released from the liposomes, the greater the risk of toxicity (illustrated by the red line in Fig. 10). A slower release from an otherwise equal dose would result in drug concentrations well within the therapeutic window (green line, Fig. 10).

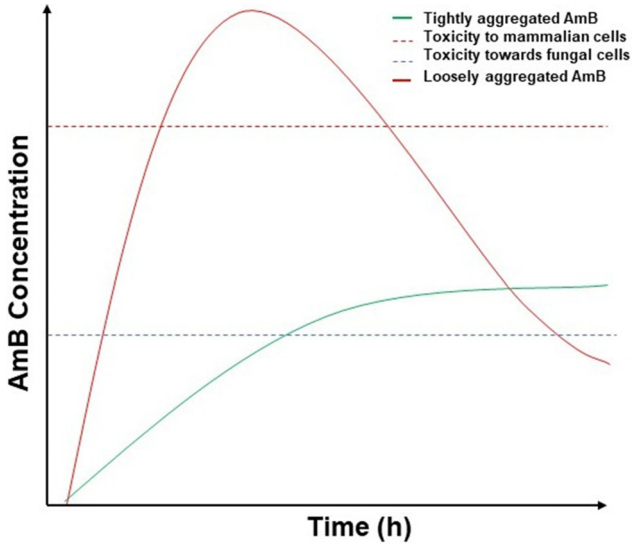

Fig. 10 – Perceived differences in systemic drug concentration patterns in slow release (*e.g.*, cured, green) and fast release (*e.g.*, uncured, red).

3.4. *Resolving a discrepancy*

The combined correlations among aggregation, release rates, and *in vitro* toxicity further highlight a recently observed contradiction. On the one hand, curing was shown to reduce toxicity when tested *in vitro* on RBCs [30]. On the other hand, curing also increases the formation of tight aggregates with spectral features consistent with tetrameric structures. Tetrameric structures were shown to fulfill the criteria for pore-forming species [25], which should increase toxicity. The current study conforms with this situation but may also resolve this discrepancy.

This study shows that toxicity is not solely dependent on the pore-forming capacity of the aggregates in the membranes of origin (the lipid bilayer of the formulation). Additional features that affect the overall expression of toxicity are the *mode of drug delivery* to the target cell and the *stability* (to disintegration) of the aggregates in the bilayer.

Mode of drug delivery: Different mechanisms were proposed for the delivery of AmB from the liposome to the target fungal cell (or for the induction of toxicity in human cells). Potassium leakage from the target cells (an *in vitro* toxicity indicator) was shown to be induced in the absence of serum components (albumin, lipoproteins) [29,49,51,52]. Thus, fusion or adsorption of cured liposomes with the target cell would be expected to increase toxicity since higher amounts of pore-ready complexes would be delivered to the target cell membrane. Our observations show the exact opposite (Fig. 8), a reduced toxicity of the cured product, thus suggesting that liposomes do not fuse with the RBC membranes and that if they only adsorb to the cell surface, then intact (pore-forming) aggregate transfer between the membranes is not the primary drug delivery mechanism. If following curing a significant portion of the AmB consists of (tight) oligomeric structures, and since dimers had been implicated earlier as responsible for toxicity [14,19,51,60], then *in situ* dissociation of these tight aggregates must occur, for transfer between adsorbed liposomes and target cells. Once dimers and monomers become available, they could also be delivered systemically by serum lipoproteins or albumin [14,51,60]. Thus, since pore-forming aggregates in the liposome are not directly delivered intact to the target cell membrane, they must first dissociate in the bilayer before drug release.

Stability: The requirement for *in situ* dissociation of tight aggregates to generate dimers (to support non-fusion modes of delivery) should not automatically imply differences in

toxicity unless this very dissociation becomes the rate-limiting step. For the first time, this study shows that the rate of dissociation from the tight aggregates (reflected in the drug release rate constants (Table 2)) is indeed a rate-limiting step. In the fully cured specimen, the release rate constant of the tight aggregates (K_B) is 28-fold lower than that of the loose aggregates (K_A). Namely, AmB aggregates with spectral features consistent with pore-forming structures are more thermodynamically stable. This increased stability attenuates dimer/monomer availability, and since release involves these smaller-sized species, the slower dissociation results in reduced toxicity.

3.5. *Physiological relevance*

The γCD-mediated release test has been established as a useful *in vitro* test for drug release from liposomal AmB products [58]. The present study shows a relation between curing and AmB release based on this method. However, there is no γCD *in vivo*, and the release occurs at body temperature, not at 55 °C as in the assay. Therefore, the AmB release test was carried out at 37 °C with a bovine serum-supplemented medium (instead of γCD) to ascertain the curing effects on drug release under physiological conditions. AmB release into serum has been previously studied [60]. Bovine serum was used at concentrations of 50% in the IVRT buffer (without γCD). Once released from the liposome and associated with serum components, AmB absorbs like a monomer, with a peak absorbance at 415 nm (no increase in absorbance is observed in the absence of serum).

Fig. 11 shows the change in the net OD_{415} presented as release (%) (Fig. 11A) and OD_{415}/OD_{max} (Fig. 11B) for uncured and fully cured liposomal AmB specimens. The data show an increase with time of serum-associated AmB, reflecting the liposome's drug release. The results agree with the earlier IVRT findings (Fig. 4A), where AmB was released from uncured preparations much faster than fully cured specimens. It also shows that the release from the cured specimen was similar to the release from AmBisome. The difference between AmB release of cured *vs*. uncured specimens was more prominent after two days of incubation than after 5 h. In summary, data generated under more physiological conditions are consistent with those derived under the IVRT test conditions.

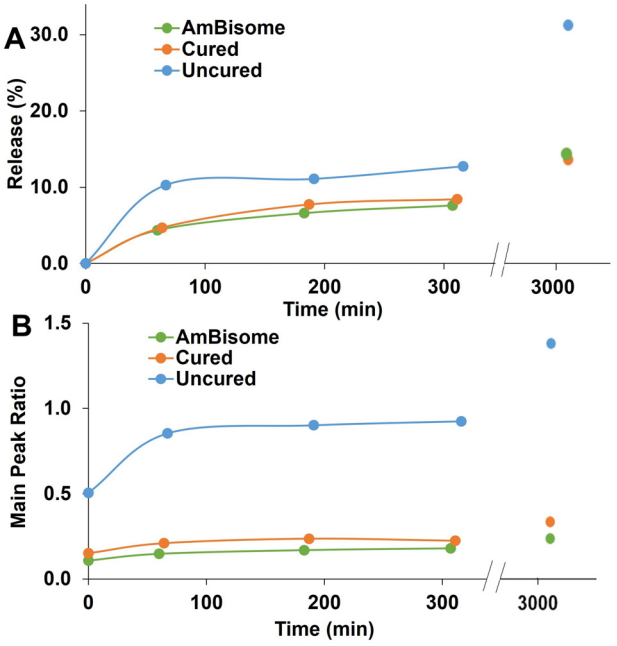

Fig. 11 – (A) Release percent and (B) peak ratio (OD_{415}/OD_{max}) of AmB released into IVRT media containing 50% bovine serum without γCD. AmBisome RLD (green), cured AmBisome-like formulation (orange) and uncured formulation (blue).

4. Conclusions

AmB liposomal preparations with the same chemical composition and manufacturing process but with a varying thermal curing step were created to examine the effect of AmB aggregation status on *in vitro* toxicity. Study results (summarized in Fig. 12) suggest that curing shifts AmB in the bilayer to more tightly aggregated forms, including the possibility for the existence of higher oligomeric forms ($n > 4$). These changes are evident by the spectral blue-shift of the main absorbance peak and a 3-fold increase in the fraction of the tightly aggregated pool. An extremely slow AmB release rate characterizes this pool. This slower release, in turn, prevents a concentration spike, thereby reducing toxicity

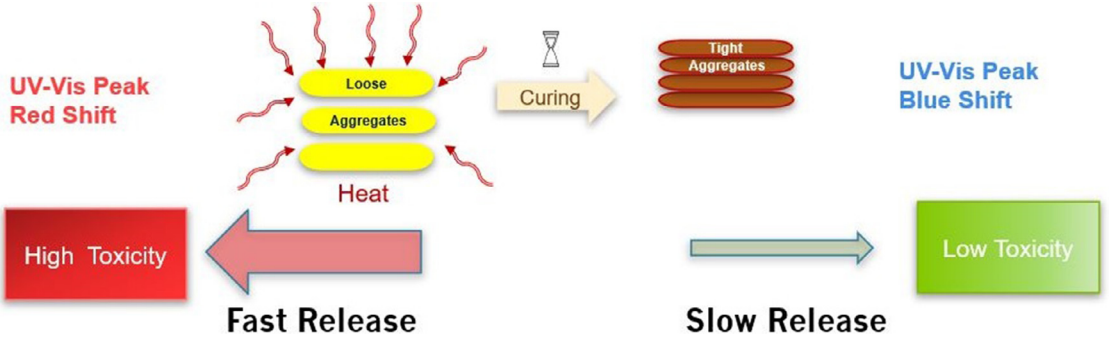

Fig. 12 – Relationships between curing, aggregation and the various characteristics of the drug product. Curing promotes tight aggregation of AmB, which in turn, slows down drug relase and reduces toxicity.

as demonstrated *in vitro*. The findings also explain how an increase in pore-forming species can be associated with low toxicity due to the rate-limiting slow dissociation of the tight aggregates that may be a prerequisite to drug release.

Conflicts of interest

The authors report no conflicts of interest. The authors alone are responsible for the content and writing of this article. This article reflects the authors' views and should not be construed to represent the FDA's views or policies.

Acknowledgments

This work was financially supported by the Office of Research and Standards, Office of Generic Drugs, CDER at the FDA (75F40120C00055).

Landrau Scientific Innovations, LLC would like to formally acknowledge the following persons and their institutions, whose assistance in this effort was invaluable. We first want to thank Mr. David Hunter of Dihydromatics, Inc. and his team for providing the Shear Jet PL-60. Their unit and technical expertise were instrumental to the success of this project. Also, we would like to thank James Jezierski, Dr. Lanu Stoddart and Harrington Hospital for their help in supplying AmBisome for both FDA projects.

REFERENCES

[1] Borowski E, Zieliński J, Ziminski T, Falkowski L, Kolodziejczyk P, et al. Chemical studies with amphotericin B. 3. The complete structure of the antibiotic. Tetrahedron Lett 1970(45):3909–14.
[2] Ernst C, Grange J, Rinnert H, Dupont G, Lematre J. Structure of amphotericin B aggregates as revealed by UV and CD spectroscopies. Biopolymers 1981;20(8):1575–88.
[3] Hemenger RP, Kaplan T, Gray LJ. Structure of amphotericin B aggregates based on calculations of optical spectra. Biopolymers 1983;22(3):911–18.
[4] Barwicz J, Gruszecki WI, Gruda I. Spontaneous organization of amphotericin B in aqueous medium. J Colloid Interface Sci 1993;158(1):71–6.
[5] Tancrède P, Barwicz J, Jutras S, Gruda I. The effect of surfactants on the aggregation state of amphotericin B. Biochim Biophys Acta 1990;1030(2):289–95.
[6] Theresa Lamy-Freund M, Schreier S, Peitzsch RM, Reed WF. Characterization and time dependence of amphotericin B: deoxycholate aggregation by quasielastic light scattering. J Pharm Sci 1991;80(3):262–6.
[7] Toledo Grijalba M, Chéron M, Borowski E, Bolard J, Schreier S. Modulation of polyene antibiotics self-association by ions from the Hofmeister series. BBA - General Subjects 2006;1760(6):973–9.
[8] Legrand P, Romero EA, Cohen BE, Bolard J. Effects of aggregation and solvent on the toxicity of amphotericin B to human erythrocytes. Antimicrob Agents Chemother 1992;36(11):2518–22.
[9] Bolard J, Seigneuret M, Boudet G. Interaction between phospholipid bilayer membranes and the polyene antibiotic amphotericin B: lipid state and cholesterol content dependence. Biochim Biophys Acta 1980;599(1):280–93.
[10] Egito LCM, Batistuzzo de Medeiros SR, Medeiros MG, Price JC, Egito EST. Evaluation of the relationship of the molecular aggregation state of amphotericin B in medium to its genotoxic potential. J Pharm Sci 2004;93(6):1557–65.
[11] Sánchez-Brunete JA, Dea MA, Rama S, Bolás F, Alunda JM, et al. Amphotericin B molecular organization as an essential factor to improve activity/toxicity ratio in the treatment of visceral leishmaniasis. J Drug Target 2004;12(7):453–60.
[12] Lamy-Freund MT, Ferreira VF, Schreier S. Polydispersity of aggregates formed by the polyene antibiotic amphotericin B and deoxycholate. A spin label study. Biochim Biophys Acta 1989;981(2):207–12.
[13] Mazerski J, Grzybowska J, Borowski E. Influence of net charge on the aggregation and solubility behaviour of amphotericin B and its derivatives in aqueous media. Eur Biophys J 1990;18(3):159–64.
[14] Brajtburg J, Bolard J. Carrier effects on biological activity of amphotericin B. Clin Microbiol Rev 1996;9(4):512–31.
[15] Lambing HE, Wolf BD, Hartsel SC. Temperature effects on the aggregation state and activity of amphotericin B. Biochim Biophys Acta 1993;1152(1):185–8.
[16] Gaboriau F, Chéron M, Petit C, Bolard J. Heat-induced superaggregation of amphotericin B reduces its *in vitro* toxicity: a new way to improve its therapeutic index. Antimicrob Agents Chemother 1997;41(11):2345–51.
[17] Gaboriau F, Chéron M, Leroy L, Bolard J. Physico-chemical properties of the heat-induced 'superaggregates' of amphotericin B. Biophys Chem 1997;66(1):1–12.
[18] Chapados C, Barwicz J, Gruda I. Separation of overlapping spectra from evolving systems using factor analysis.: 2. Amphotericin B in aqueous propanol and in aqueous lauroyl sucrose. Biophys Chem 1994;51(1):71–80.
[19] Wójtowicz K, Gruszecki WI, Walicka M, Barwicz J. Effect of amphotericin B on dipalmitoylphosphatidylcholine membranes: calorimetry, ultrasound absorption and monolayer technique studies. Biochim Biophys Acta 1998;1373(1):220–6.
[20] Janoff AS, Boni LT, Popescu MC, Minchey SR, Cullis PR, et al. Unusual lipid structures selectively reduce the toxicity of amphotericin B. Proc Natl Acad Sci USA 1988;85(16):6122–6.
[21] Gagoś M, Koper R, Gruszecki WI. Spectrophotometric analysis of organisation of dipalmitoylphosphatidylcholine bilayers containing the polyene antibiotic amphotericin B. BBA - Biomembranes 2001;1511(1):90–8.
[22] Yamaji N, Matsumori N, Matsuoka S, Oishi T, Murata M. Amphotericin B dimers with bisamide linkage bearing powerful membrane-permeabilizing activity. Org Lett 2002;4(12):2087–9.
[23] Starzyk J, Gruszecki M, Tutaj K, Luchowski R, Szlazak R, et al. Self-association of amphotericin B: spontaneous formation of molecular structures responsible for the toxic side effects of the antibiotic. J Phys Chem B 2014;118(48):13821–32.
[24] Grant CW, Hamilton KS, Hamilton KD, Barber KR. Physical biochemistry of a liposomal amphotericin B mixture used for patient treatment. Biochim Biophys Acta 1989;984(1):11–20.
[25] Wasko P, Luchowski R, Tutaj K, Grudzinski W, Adamkiewicz P, et al. Toward understanding of toxic side effects of a polyene antibiotic amphotericin B: fluorescence spectroscopy reveals widespread formation of the specific supramolecular structures of the drug. Mol Pharm 2012;9(5):1511–20.
[26] Torrado JJ, Espada R, Ballesteros MP, Torrado-Santiago S. Amphotericin B formulations and drug targeting. J Pharm Sci 2008;97(7):2405–25.

[27] Gruszecki WI, Gagoś M, Hereć M. Dimers of polyene antibiotic amphotericin B detected by means of fluorescence spectroscopy: molecular organization in solution and in lipid membranes. J Photochem Photobiol B 2003;69(1):49–57.
[28] Espada R, Valdespina S, Alfonso C, Rivas G, Ballesteros MP, et al. Effect of aggregation state on the toxicity of different amphotericin B preparations. Int J Pharm 2008;361(1):64–9.
[29] Baas B, Kindt K, Scott A, Scott J, Mikulecky P, et al. Activity and kinetics of dissociation and transfer of amphotericin B from a novel delivery form. AAPS PharmSci 1999;1(3):E10.
[30] Rivnay B, Wakim J, Avery K, Petrochenko P, Myung JH, et al. Critical process parameters in manufacturing of liposomal formulations of amphotericin B. Int J Pharm 2019;565:447–57.
[31] van Etten EW, van Vianen W, Roovers P, Frederik P. Mild heating of amphotericin B-desoxycholate: effects on ultrastructure, *in vitro* activity and toxicity, and therapeutic efficacy in severe candidiasis in leukopenic mice. Antimicrob Agents Chemother 2000;44(6):1598–603.
[32] Stoodley R, Wasan KM, Bizzotto D. Fluorescence of amphotericin B-deoxycholate (fungizone) monomers and aggregates and the effect of heat-treatment. Langmuir 2007;23(17):8718–25.
[33] Chéron M, Petit C, Bolard J, Gaboriau F. Heat-induced reformulation of amphotericin B-deoxycholate favours drug uptake by the macrophage-like cell line J774. J Antimicrob Chemother 2003;52(6):904–10.
[34] Serrano D, Ballesteros M, Schatzlein A, Torrado J, Uchegbu I. Amphotericin B formulations – the possibility of generic competition. Pharma Nanotechnol 2013;1:250–8.
[35] Zia Q, Azhar A, Kamal MA, Aliev G, Owais M, et al. Super aggregated form of Amphotericin B: a novel way to increase its therapeutic index. Curr Pharm Des 2016;22(7):792–803.
[36] Kang JY, Gao J, Shin DH, Alvarez C, Zhong W, et al. Pharmacokinetics and renal toxicity of monomeric amphotericin B in rats after a multiple dose regimen. Pharm Nanotechnol 2016;4(1):16–23.
[37] Petit C, Yardley V, Gaboriau F, Bolard J, Croft SL. Activity of a heat-induced reformulation of amphotericin B deoxycholate (fungizone) against Leishmania donovani. Antimicrob Agents Chemother 1999;43(2):390–2.
[38] Bartlett K, Yau E, SCl Hartse, Hamer A, Tsai G, et al. Effect of heat-treated amphotericin B on renal and fungal cytotoxicity. Antimicrob Agents Chemother 2004;48(1):333–6.
[39] Liu H, Rivnay B, Avery K, Myung JH, Kozak D, et al. Optimization of the manufacturing process of a complex amphotericin B liposomal formulation using quality by design approach. Int J Pharm 2020;585.
[40] Tremblay C, Barza M, Fiore C, Szoka F. Efficacy of liposome-intercalated amphotericin B in the treatment of systemic candidiasis in mice. Antimicrob Agents Chemother 1984;26(2) 170-13.
[41] Adler-moore JP, Proffitt RT. Development, characterization, efficacy and mode of action of ambisome, a unilamellar liposomal formulation of amphotericin B. J Liposome Res 1993;3(3):429–50.
[42] Panosian CB, Barza M, Szoka F, Wyler DJ. Treatment of experimental cutaneous leishmaniasis with liposome-intercalated amphotericin B. Antimicrob Agents Chemother 1984;25(5):655–6.
[43] Lim CB, Abuzar SM, Karn PR, Cho W, Park HJ, et al. Preparation, characterization, and *in vivo* pharmacokinetic study of the supercritical fluid-processed liposomal amphotericin B. Pharmaceutics 2019;11(11):589.
[44] Juliano RL, Lopez-Berestein G, Hopfer R, Mehta R, Mehta K, et al. Selective toxicity and enhanced therapeutic index of liposomal polyene antibiotics in systemic fungal infections. Ann N Y Acad Sci 1985;446:390–402.
[45] Lopez-Berestein G, Mehta R, Hopfer R, Mehta K, Hersh EM, et al. Effects of sterols on the therapeutic efficacy of liposomal amphotericin B in murine candidiasis. Cancer Drug Deliv 1983;1(1):37–42.
[46] Szoka FC, Milholland D, Barza M. Effect of lipid composition and liposome size on toxicity and *in vitro* fungicidal activity of liposome-intercalated amphotericin B. Antimicrob Agents Chemother 1987;31(3):421–9.
[47] Payne NI, Cosgrove RF, Green AP, Liu L. *In-vivo* studies of amphotericin B liposomes derived from proliposomes: effect of formulation on toxicity and tissue disposition of the drug in mice. J Pharm Pharmacol 1987;39(1):24–8.
[48] Sculier JP, Coune A, Meunier F, Brassinne C, Laduron C, et al. Pilot study of amphotericin B entrapped in sonicated liposomes in cancer patients with fungal infections. Eur J Cancer Clin Oncol 1988;24(3):527–38.
[49] Jensen GM, Skenes CR, Bunch TH, Weissman CA, Amirghahari N, et al. Determination of the relative toxicity of amphotericin B formulations: a red blood cell potassium release assay. Drug Deliv 1999;6(2):81–8.
[50] Peterson RP, Benz SK, Whyte BS, Hartsel SC. A kinetic method for measuring functional delivery of amphotericin B by drug delivery systems. Biochim Biophys Acta 1991;1064(1):165–8.
[51] Bolard J, Legrand P, Heitz F, Cybulska B. One-sided action of amphotericin B on cholesterol-containing membranes is determined by its self-association in the medium. Biochemistry 1991;30(23):5707–15.
[52] Yu BG, Okano T, Kataoka K, Sardari S, Kwon GS. *In vitro* dissociation of antifungal efficacy and toxicity for amphotericin B-loaded poly(ethylene oxide)-block-poly(beta benzyl L aspartate) micelles. J Control Rel 1998;56(1–3):285–91.
[53] Serrano DR, Hernández L, Fleire L, González-Alvarez I, Montoya A, et al. Hemolytic and pharmacokinetic studies of liposomal and particulate amphotericin B formulations. Int J Pharm 2013;447(1):38–46.
[54] Grela E, Zdybicka-Barabas A, Pawlikowska-Pawlega B, Cytrynska M, Wlodarczyk M, et al. Modes of the antibiotic activity of amphotericin B against Candida albicans. Sci Rep 2019;9(1):17029.
[55] Butler WT, Cotlove E. Increased permeability of human erythrocytes induced by amphotericin B. J Infect Dis 1971;123(4):341–50.
[56] Mehta R, Lopez-Berestein G, Hopfer R, Mills K, Juliano RL. Liposomal amphotericin B is toxic to fungal cells but not to mammalian cells. Biochim Biophys Acta 1984;770(2):230–4.
[57] G.W. James D Dutcher, WILLIAM G.O.L.D., Joseph F Pagano, Vandeputte John. Amphotericin B, Its Production, and Its Salts. USA, US19540478014 [P]. 1959-10-13.
[58] Tang J, Srinivasan S, Yuan W, Ming R, Liu Y, et al. Development of a flow-through USP 4 apparatus drug release assay for the evaluation of amphotericin B liposome. Eur J Pharm Biopharm 2019;134:107–16.
[59] Legrand P, Chéron M, Leroy L, Bolard J. Release of amphotericin B from delivery systems and its action against fungal and mammalian cells. J Drug Target 1997;4(5):311–19.
[60] Hartsel SC, Baas B, Bauer E, Foree LT, Kindt JK, et al. Heat-induced superaggregation of amphotericin B modifies its interaction with serum proteins and lipoproteins and stimulation of TNF-alpha. J Pharm Sci 2001;90(2):124–33.